Ocean Modelling 23 (2008) 49–58

Contents lists available at ScienceDirect

Ocean Modelling

journal homepage: www.elsevier.com/locate/ocemod

The effect of ageostrophy on the stability of vortices in a two-layer ocean

E.S. Benilov *, J.D. Flanagan

Department of Mathematics, University of Limerick, Plassey Technological Park, Limerick, Ireland

ARTICLE INFO

Article history:
Received 4 October 2007
Received in revised form 23 March 2008
Accepted 24 March 2008
Available online 4 April 2008

Keywords:
Eddies
Vortices
Two-layer model
Stability

ABSTRACT

We present a numerical study of stability of two-layer isolated vortices on the *f*-plane with respect to normal modes, i.e. disturbances with harmonic dependence on the azimuthal angle and time. Two types of vortices are considered: compensated vortices (for which the lower-layer is at rest), and vortices with uniform potential vorticity in the lower layer (for which a weak co-rotating circulation exists in the lower layer). It is demonstrated that, if the upper-layer is *thin*, the numerical results agree with the earlier asymptotic results namely, that the latter type of vortex is stable within a wide range of parameter and, thus, can account for the observed longevity of oceanic eddies. Compensated vortices, in turn, are typically unstable, with ageostrophic effects strengthening the instability for cyclones and weakening it for anticyclones.

We also demonstrate that, under relatively loose assumptions, Ripa's [Ripa, P., 1989. On the stability of ocean vortices. In: Nihoul, J.C.J., Jamart, B.M. (Eds.), Mesoscale/Synoptic Coherent Structures in Geophysical Turbulence: Proceedings of the 20th International Liège Colloquium on Ocean Hydrodynamics, Elsevier Oceanography Series, vol. 50. Elsevier, Amsterdam, p. 167] stability criterion does not hold for oceanic vortices with realistic parameters.

1. Introduction

The discrepancy between theoretical and observational studies of oceanic eddies has been identified almost 30 years ago. On the one hand, most theoretical work on the subject (e.g. Ikeda, 1981; Flierl, 1988; Helfrich and Send, 1988; Carton and McWilliams, 1989; Ripa, 1992; Killworth et al., 1997; Benilov et al., 1998; Baey and Carton, 2002; Benilov, 2003; Katsman et al., 2003; Benilov, 2005) suggest that eddies are unstable with respect to small perturbations; on the other hand, observations (e.g. Lai and Richardson, 1977) indicate that eddies exist for years. A potential solution of the paradox was put forward by Dewar and Killworth (Dewar and Killworth, 1995), who considered a two-layer ocean with a vortex in the upper-layer and a co-rotating circulation in the lower-layer. It turned out that even a relatively weak 'deep flow' may stabilize the eddy. This effect has been later examined for other vortex shapes by Katsman et al. (2003), but no profile except for the Gaussian one would become entirely stable (although, in all examples considered, a co-rotating deep flow would reduce the growth rate).

Note that (Dewar and Killworth, 1995; Katsman et al., 2003) assumed that the deep circulation has the same shape as the upper-layer vortex. A different approach was used in Benilov (2004), where it was demonstrated that *all* vortices, not just the Gaussian one, are stabilized by the deep flow corresponding to *uniform potential vorticity (PV) in the lower-layer*. The following mechanism of stabilization was suggested: an unstable normal mode can be interpreted as two phase-locked vorticity waves in the upper and lower layers, existing due to the PV gradient and travelling around the vortex as they grow. If, however, the lower-layer PV field is uniform, it cannot support vorticity waves, and baroclinic instability (for which both waves are needed) is inhibited.

Furthermore (Benilov, 2004) argued that deep flow with uniform PV arises naturally below oceanic eddies, as suggested by the fact that most of them are shed by unstable frontal currents. Accordingly, when a vortex moves away from the current and arrives to a new location, the PV field below it cannot change and remains equal to its initial, background value.

Note that the main focus of Benilov (2004) was quasigeostrophic (QG) vortices, which were examined both asymptotically (for the case of thin upper-layer) and numerically. With regards to *a*geostrophic vortices, it was only argued asymptotically that, if they are thin, their stability properties should be similar to those of their QG counterparts. Note, however, that the ageostrophic approximation admits internal gravity waves, and these can cause an instability which is simply too weak to be 'spotted' by the leading-order analysis presented in Benilov (2004).

The present note aims to examine the ageostrophic approximation numerically, with an accuracy guaranteeing that all instabilities are detected. We use the simplest model of two-layer ocean on the *f*-plane. In Section 2, the problem of vortex stability is

* Corresponding author. Tel.: +353 61 213 146.
E-mail address: eugene.benilov@ul.ie (E.S. Benilov).

1463-5003/$ - see front matter © 2008 Elsevier Ltd. All rights reserved.
doi:10.1016/j.ocemod.2008.03.004

formulated mathematically. In Sections 3 and 4, we examine the stability of compensated vortices (for which the lower-layer is at rest) and vortices with uniform PV in the lower-layer, respectively. Finally, in Section 5, we demonstrate that, under fairly loose assumptions, Ripa's criterion (Ripa, 1989, 1991) does not work for isolated ageostrophic vortices (which explains why this and most other papers on the subject are based on the numerical, rather than analytical, approach).

2. Formulation

Consider a two-layer ocean with rigid lid and flat bottom, where the densities and mean depths of the layers are ρ_j and H_{*j} ($j = 1,2$ correspond to the upper and lower-layer, respectively, and asterisks imply that the corresponding quantity is dimensional). We shall also introduce the upper-layer deformation radius

$$L_\mathrm{d} = \frac{\sqrt{g' H_{*1}}}{f_0},$$

where $g' = g(\rho_2 - \rho_1)/\rho_2$ is the reduced acceleration due to gravity and f_0 is the Coriolis parameter.

In a two-layer ageostrophic ocean, the flow is characterized by the layers' depths h_{*j}, pressures p_{*j}, the radial velocities u_{*j}, and the azimuthal velocities v_{*j}. These variables depend on the time t_* and polar coordinates (the radial variable r_* and azimuthal angle θ_*).

Next, introduce the following non-dimensional variables:

$$t = f_0 t_*, \quad r = \frac{r_*}{L_\mathrm{d}}, \quad \theta = \theta_*,$$

$$u_j = \frac{u_{*j}}{f_0 L_\mathrm{d}}, \quad v_j = \frac{v_{*j}}{f_0 L_\mathrm{d}}, \quad h_j = \frac{h_{*j}}{H_{*j}}, \quad p_j = \frac{p_{*j}}{\rho_2 g' H_{*1}}.$$

Then, the non-dimensional equations governing two-layer ageostrophic vortices on the f-plane are

$$\frac{\partial u_j}{\partial t} + u_j \frac{\partial u_j}{\partial r} + \frac{1}{r} v_j \left(\frac{\partial u_j}{\partial \theta} - v_j \right) + \frac{\partial p_j}{\partial r} = v_j, \tag{1}$$

$$\frac{\partial v_j}{\partial t} + u_j \frac{\partial v_j}{\partial r} + \frac{1}{r} v_j \left(\frac{\partial v_j}{\partial \theta} + u_j \right) + \frac{1}{r} \frac{\partial p_j}{\partial \theta} = -u_j, \tag{2}$$

$$r \frac{\partial h_j}{\partial t} + \frac{\partial}{\partial r}(r u_j h_j) + \frac{\partial}{\partial \theta}(v_j h_j) = 0, \tag{3}$$

$$p_2 = p_1 - h_1, \quad \varepsilon h_1 + h_2 = 1 + \varepsilon, \tag{4}$$

where

$$\varepsilon = \frac{H_{*1}}{H_{*2}}.$$

In what follows, Eqs. (1)–(4) will be reduced to a simpler set describing linear disturbances with harmonic dependence on the azimuthal and time variables. Such sets have been derived before (Dewar and Killworth, 1995; Baey and Carton, 2002), therefore, we shall keep the details to a minimum.

Following the usual scheme of linear stability analysis, we consider a steady vortex and small disturbance,

$$u_j(r,\theta,t) = u_j'(r,\theta,t), \quad v_j(r,\theta,t) = V_j(r) + v_j'(r,\theta,t), \tag{5}$$

$$p_j(r,\theta,t) = P_j(r) + p_j'(r,\theta,t), \quad h_j(r,\theta,t) = H_j(r) + h_j'(r,\theta,t), \tag{6}$$

where the vortex satisfies the cyclostrophic, hydrostatic, and kinematic relations,

$$\frac{\mathrm{d}P_j}{\mathrm{d}r} = V_j + \frac{1}{r} V_j^2, \quad P_2 = P_1 - H_1, \quad \varepsilon H_1 + H_2 = 1 + \varepsilon. \tag{7}$$

It is also implied that

$$H_j \to 1, \quad V_j \to 0 \text{ as } r \to \infty. \tag{8}$$

Substituting (5)–(7) into (1)–(4) and omitting nonlinear terms, we obtain

$$\frac{\partial u_j'}{\partial t} + \frac{1}{r} V_j \left(\frac{\partial u_j'}{\partial \theta} - v_j' \right) - \frac{1}{r} v_j' V_j + \frac{\partial p_j'}{\partial r} = v_j', \tag{9}$$

$$\frac{\partial v_j'}{\partial t} + u_j' \frac{\mathrm{d}V_j}{\mathrm{d}r} + \frac{1}{r} V_j \left(\frac{\partial v_j'}{\partial \theta} + u_j' \right) + \frac{1}{r} \frac{\partial p_j'}{\partial \theta} = -u_j', \tag{10}$$

$$r \frac{\partial h_j'}{\partial t} + \frac{\partial}{\partial r}(r u_j' H_j) + \frac{\partial}{\partial \theta}\left(V_j h_j' + v_j' H_j \right) = 0, \tag{11}$$

$$p_2' = p_1' - h_1', \quad \varepsilon h_1' + h_2' = 0. \tag{12}$$

We are interested in normal modes, i.e., solutions with harmonic dependence on the time and azimuthal angle,

$$u_j' = Re[\hat{u}_j(r) \mathrm{e}^{\mathrm{i}k\theta - \mathrm{i}\omega t}], \quad v_j' = Re[\hat{v}_j(r) \mathrm{e}^{\mathrm{i}k\theta - \mathrm{i}\omega t}], \tag{13}$$

$$p_j' = Re[\hat{p}_j(r) \mathrm{e}^{\mathrm{i}k\theta - \mathrm{i}\omega t}], \quad h_j' = Re[\hat{h}_j(r) \mathrm{e}^{\mathrm{i}k\theta - \mathrm{i}\omega t}], \tag{14}$$

where ω and k are the frequency and azimuthal wavenumber. Substitution of (13) and (14) into (9)–(12) yields (hats omitted)

$$\mathrm{i}\left(\frac{k}{r} V_j - \omega \right) u_j - \left(1 + \frac{2}{r} V_j \right) v_j + \frac{\mathrm{d}p_j}{\mathrm{d}r} = 0, \tag{15}$$

$$\mathrm{i}\left(\frac{k}{r} V_j - \omega \right) v_j + \left(1 + \frac{1}{r} V_j + \frac{\mathrm{d}V_j}{\mathrm{d}r} \right) u_j + \frac{\mathrm{i}k}{r} p_j = 0, \tag{16}$$

$$\mathrm{i}\left(\frac{k}{r} V_j - \omega \right) h_j + \frac{1}{r} \frac{\mathrm{d}}{\mathrm{d}r}(r H_j u_j) + \frac{\mathrm{i}k}{r} H_j v_j = 0, \tag{17}$$

$$p_2 = p_1 - h_1, \quad \varepsilon h_1 + h_2 = 0. \tag{18}$$

It is convenient to reduce (15)–(18) to two equations for $p_{1,2}$. Using (15) and (16) to express u_j, v_j through p_j,

$$u_j = -\mathrm{i} \frac{\left(\frac{k}{r} V_j - \omega \right) \frac{\mathrm{d}p_j}{\mathrm{d}r} + \left(1 + \frac{2}{r} V_j \right) \frac{k}{r} p_j}{\left(1 + \frac{1}{r} V_j + \frac{\mathrm{d}V_j}{\mathrm{d}r} \right) \left(1 + \frac{2}{r} V_j \right) - \left(\frac{k}{r} V_j - \omega \right)^2},$$

$$v_j = \frac{\left(1 + \frac{1}{r} V_j + \frac{\mathrm{d}V_j}{\mathrm{d}r} \right) \frac{\mathrm{d}p_j}{\mathrm{d}r} + \left(\frac{k}{r} V_j - \omega \right) \frac{k}{r} p_j}{\left(1 + \frac{1}{r} V_j + \frac{\mathrm{d}V_j}{\mathrm{d}r} \right) \left(1 + \frac{2}{r} V_j \right) - \left(\frac{k}{r} V_j - \omega \right)^2},$$

we substitute these expressions into (17) and, after cumbersome calculations, obtain

$$\frac{\mathrm{d}}{\mathrm{d}r}\left(r F_j \frac{\mathrm{d}p_j}{\mathrm{d}r} \right) + \left\{ \frac{\frac{\mathrm{d}}{\mathrm{d}r}\left[k \left(1 + \frac{2}{r} V_j \right) F_j \right]}{\frac{k}{r} V_j - \omega} - \frac{k^2}{r} F_j \right\} p_j - r h_j = 0, \tag{19}$$

where

$$F_j = \frac{H_j}{\left(1 + \frac{1}{r} V_j + \frac{\mathrm{d}V_j}{\mathrm{d}r} \right) \left(1 + \frac{2}{r} V_j \right) - \left(\frac{k}{r} V_j - \omega \right)^2}. \tag{20}$$

To 'close' these equations, express h_j in terms of p_j from (12),

$$h_1 = p_1 - p_2, \quad h_2 = \varepsilon(p_2 - p_1). \tag{21}$$

Finally, we impose the usual boundary conditions at the center of the vortex and infinity,

$$p_j \to 0 \quad \text{as} \quad r \to 0, \infty. \tag{22}$$

Eqs. (19)–(22) form an eigenvalue problem, where ω is the eigenvalue. If $\mathrm{Im}\omega > 0$, the vortex is unstable.

Observe that, for marginally stable solutions (such that $\mathrm{Im}\omega = 0$), Eq. (19) has a singularity at the critical level, i.e., at a point $r = r_c$ where the angular velocity in one of the layers matches the angular phase velocity of the eigenmode,

$$\frac{1}{r}V_j = \frac{\omega}{k} \quad \text{at} \quad r = r_c. \tag{23}$$

In addition, there can be a singularity, at a point $r = r_c'$ where

$$\left(1 + \frac{1}{r}V_j + \frac{\mathrm{d}V_j}{\mathrm{d}r}\right)\left(1 + \frac{2}{r}V_j\right) - \left(\frac{k}{r}V_j - \omega\right)^2 = 0 \quad \text{at} \quad r = r_c', \tag{24}$$

and one of the functions F_j becomes infinite. Singularities of type (24) will be referred to as *critical levels of the second kind*. Note that they never occur in the QG approximation, under which $|V_j| \sim |\omega| \ll 1$, and the left-hand side of (24) never vanishes:

$$\left(1 + \frac{1}{r}V_j + \frac{\mathrm{d}V_j}{\mathrm{d}r}\right)\left(1 + \frac{2}{r}V_j\right) - \left(\frac{k}{r}V_j - \omega\right)^2 \approx 1.$$

3. Compensated vortices

Let the vortex be localized in the upper-layer, with the lower-layer being at rest,

$$P_2 = 0. \tag{25}$$

In this case (7) yields

$$P_1 = H_1, \tag{26}$$

$$V_1 = \frac{1}{2}\left(\sqrt{r^2 + 4r\frac{\mathrm{d}H_1}{\mathrm{d}r}} - r\right), \quad V_2 = 0, \quad H_2 = 1 - \varepsilon(H_1 - 1). \tag{27}$$

Thus, all parameters of the vortex are determined by a single function, $H_1(r)$.

3.1. Gaussian vortices

We shall first consider vortices with a Gaussian profile,

$$H_1 = 1 + \Delta H \exp\left(-\frac{r^2}{2R^2}\right), \tag{28}$$

where R and ΔH are the non-dimensional radius and amplitude of the vortex, normalized by the upper-layer deformation radius and the mean thickness of the upper layer, respectively. Two examples of Gaussian vortices, a cyclone and an anticyclone, are shown in Fig. 1. Since we must assume $H_{1,2} > 0$ and $\mathrm{Im}V_1 = 0$, it follows from (27) that the parameters of the vortex should satisfy the following restrictions,

$$-1 \leqslant \Delta H \leqslant \frac{1}{\varepsilon}, \tag{29}$$

$$R^2 \geqslant 4\Delta H. \tag{30}$$

Physically, condition (30) ensures that the Coriolis force can hold the vortex (anticyclone) together by balancing the centrifugal force plus hydrostatic pressure gradient. Note also that, for cyclones ($\Delta H < 0$), (30) holds automatically.

Thus, the stability properties of the Gaussian vortex profile can be characterized by the corresponding marginal stability (MS) surface in the (ε, R, ΔH) parameter space, subject to restrictions (29) and (30). In this paper, the MS surface is described using its cross-sections $\Delta H = $ const. on the (ε, R)-plane.

Before examining the general case, we shall briefly review the corresponding QG limit, $\Delta H \to 0$ (examined in Benilov (2003)). In this case, cyclones and anticyclones have identical stability properties, which are illustrated in Fig. 2. First of all, observe that, if a

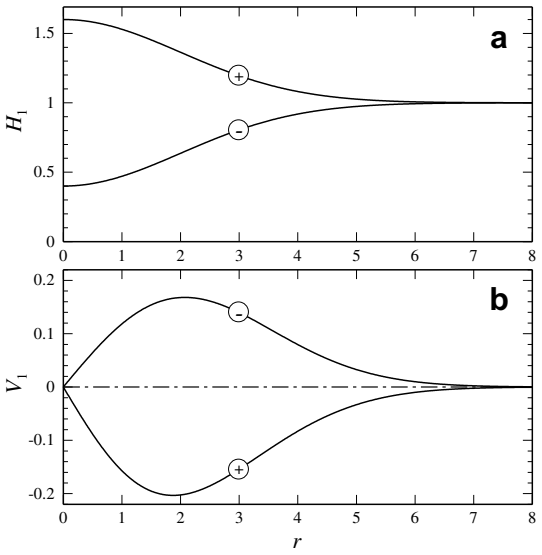

Fig. 1. Examples of compensated Gaussian vortices (25)–(28) with $\Delta H = \pm 0.6$, $R = 2$ (the cyclone/anticyclone are marked with −/+, respectively). (a) $H_1(r)$; (b) $V_1(r)$.

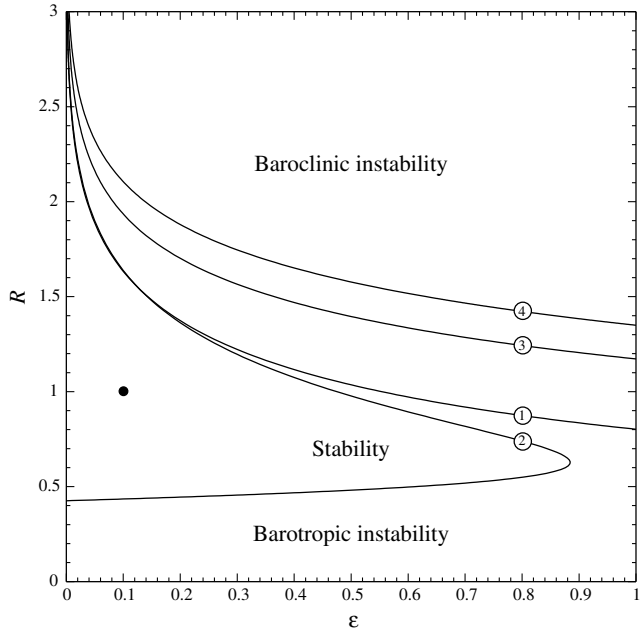

Fig. 2. The stability properties of Gaussian quasigeostrophic ($\Delta H \to 0$) vortices. The marginal stability curves are marked with the corresponding values of the azimuthal wavenumber k.

vortex is stable with respect to $k = 2$, it is also stable with respect to all other k – which makes the second azimuthal mode the most important one.

In order to understand the mechanism of instability, consider a 'reference' vortex with, say, $\varepsilon = 0.1$ and $R = 1$ (it is shown in Fig. 2 by a black dot). In this case, horizontal and vertical shear appear to 'cancel' each other, preventing the vortex from being unstable either barotropically or baroclinically. For increasing R, however, the horizontal shear weakens and the 'unopposed' vertical shear destabilizes the vortex (which is why the corresponding region in Fig. 2 is labelled "*baroclinic* instability"). For smaller R, in turn, the horizontal shear becomes too strong for the vertical shear to contain it, and the vortex becomes unstable *barotropically*. Note

also that all but the second azimuthal modes are barotropically stable.

The aim of this subsection is to examine how the above picture is affected by ageostrophic effects.

First, we shall illustrate the stability properties of the Gaussian profile (28) by numerical solutions of the eigenvalue problem (19)–(22). To compute the MS curves, we had to deal with singularities caused by critical levels (23), which were 'by-passed' by extending the path of integration into the plane of complex r (as done previously in Benilov (2003, 2004) for QG vortices).

It turns out that, for compensated *cyclones* ($\Delta H < 0$), ageostrophy is a destabilizing factor. Indeed, as illustrated for $k = 2$ in Fig. 3a, an increase in vortex amplitude causes rapid contraction of the region of stability. What happens with compensated *anticyclones*, in turn, is illustrated in Fig. 3b. On the one hand, the region of stability expands slightly towards larger vortices (which agrees with conclusions of Baey and Carton (2002)); on the other hand, a large area is excluded where condition (30) does not hold (i.e., these vortices do not exist). As a result, the region of stability for anticyclones contracts overall, and does so even faster than that for cyclones. Observe also that the stability properties of other azimuthal modes are similar, for both cyclones and anticyclones (as illustrated for $k = 1$ in Fig. 4).

Finally, we shall discuss the position of upper-layer critical levels for marginally stable vortices (compensated vortices do not have critical levels in the lower-layer). The usual critical level is always located at the periphery of the vortex, and we can 'bend' the path of integration into the complex plane to by-pass it. Critical levels of the second type, in turn, normally occur on the imaginary axis of the complex r plane – hence, they do not lie in the path of integration and do not cause difficulties. When, however, the MS curve intersects the 'existence curve' (see Fig. 3b or Fig. 4b), the critical level of the second kind happens to coincide with the center

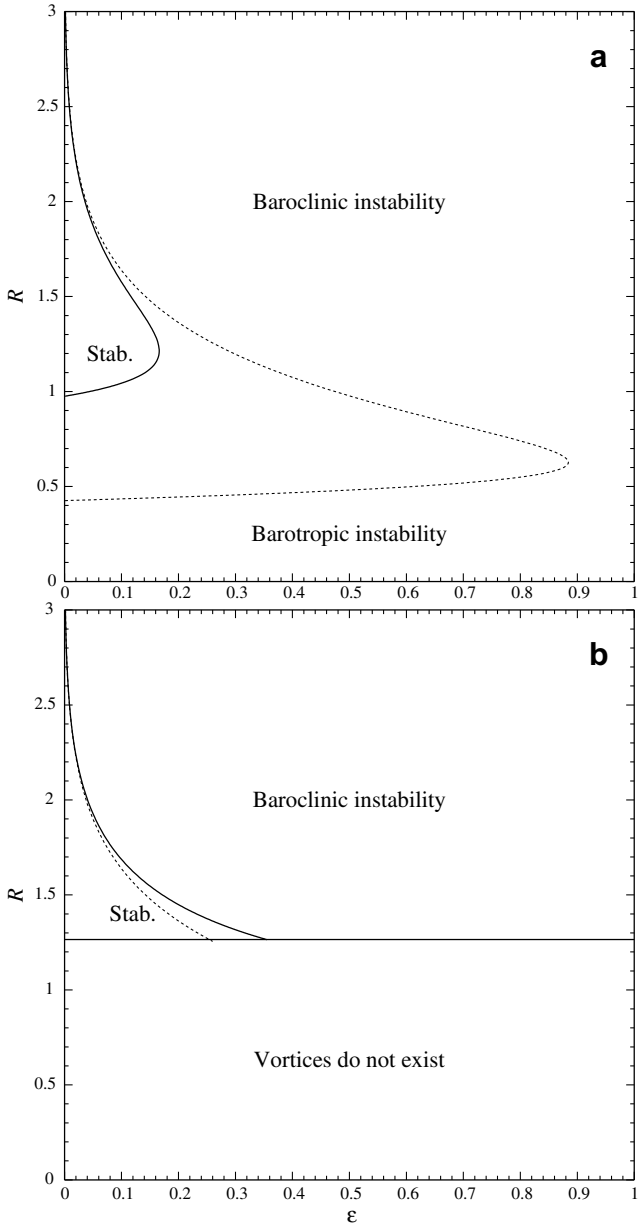

Fig. 3. The marginal stability curve for Gaussian ageostrophic vortices, for the second azimuthal mode ($k = 2$). The dotted line shows the corresponding quasigeostrophic ($\Delta H \to 0$) curve. (a) $\Delta H = -0.4$ (cyclones); (b) $\Delta H = 0.4$ (anticyclones), the horizontal line shows constraint (30).

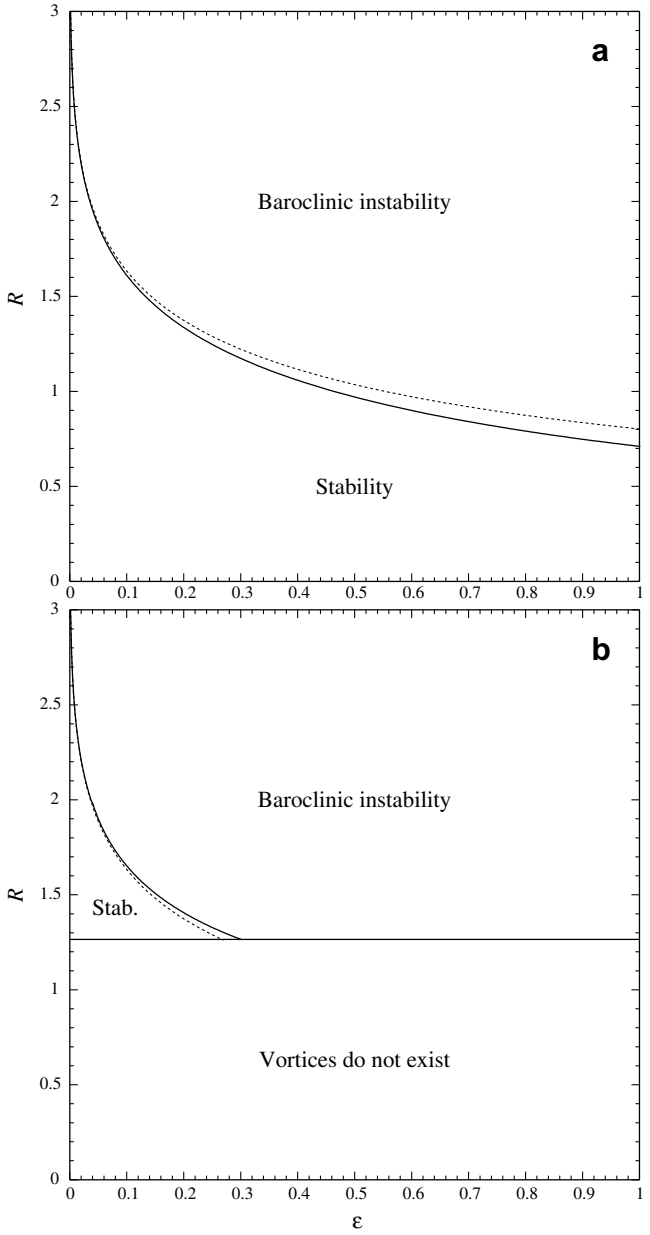

Fig. 4. The same as in Fig. 3, but for $k = 1$.

of the vortex (this is just a numerical observation, not a theorem). Since one of the boundary conditions is set at the origin, we cannot bend the path of integration around it. As a result, the singularity associated with the critical level of the second kind does not allow one to compute the stability properties of the corresponding vortex.

This difficulty has been dealt with by extrapolating the MS curve: the point where it *intersects* the existence curve was predicted using the results computed while *approaching* it.

3.2. Comparison with asymptotic results

Note that most oceanic eddies are localized in a thin layer, either near the ocean's surface or bottom, or in the thermocline. Accordingly, an asymptotic theory based on the assumption $\varepsilon \ll 1$ has been developed for compensated vortices, both QG and ageostrophic (Benilov, 2003, 2005, respectively). Quite unexpectedly, the asymptotic criterion for baroclinic instability turned out to be independent of the vortex's amplitude, i.e., whether or not a vortex is stable depends only on its shape (but the growth rate of an unstable vortex does depend on its amplitude, of course).

In the present work, this conclusion has been verified numerically and is illustrated by Fig. 5, which shows the numerical MS curves for $k = 2$ (for which the agreement between the asymptotic and numerical results happens to be the worst) and various values of the amplitude ΔH. One should keep in mind that, firstly, results obtained in Benilov (2003, 2005) pertain to *baroclinic* instability

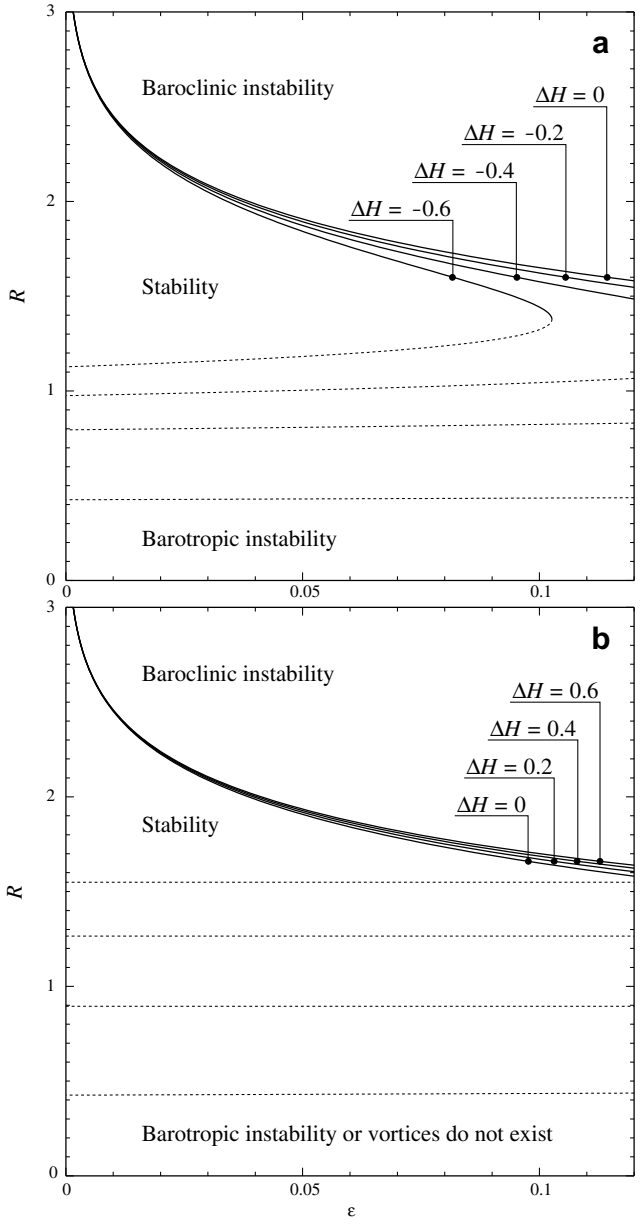

Fig. 5. The marginal stability curve for Gaussian vortices, computed for the second azimuthal mode ($k = 2$) and various values of the amplitude ΔH ($\Delta H = 0$ corresponds to the QG approximation). The dotted line shows the lower part of the curve or constraint (30) (whichever is higher). (a) Cyclones ($\Delta H < 0$); (b) anticyclones ($\Delta H > 0$).

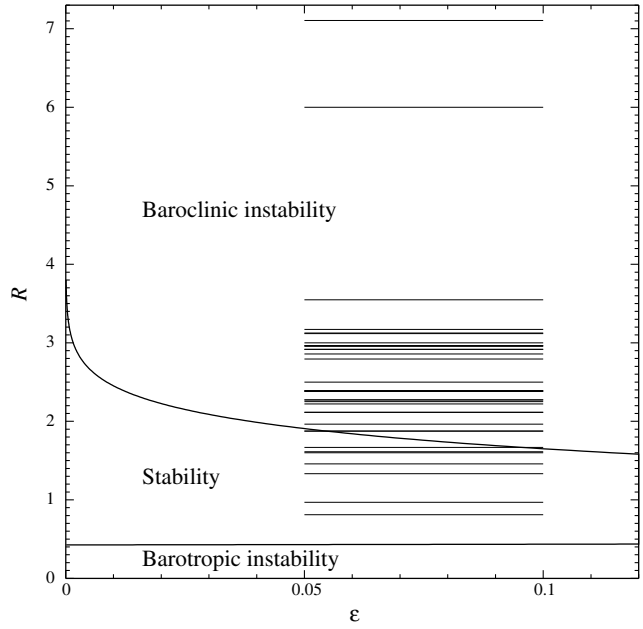

Fig. 6. The marginal stability curve for Gaussian quasigeostrophic ($\Delta H \to 0$) vortices, for the second azimuthal mode ($k = 2$). Horizontal segments show the parameters of rings catalogued in Olson (1991).

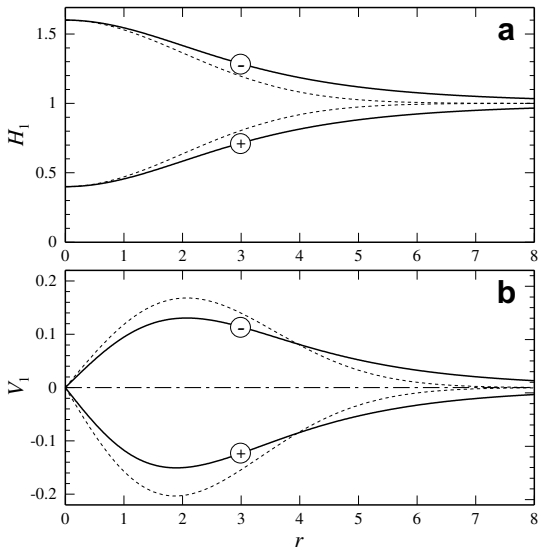

Fig. 7. Examples of compensated algebraic vortices (31) and (27) with $\Delta H = \pm 0.6$, $R = 2$ (the cyclone/anticyclone are marked with $-/+$, respectively). (a) $H_1(r)$; (b) $V_1(r)$. The dotted lines correspond to the Gaussian vortices with the same parameters.

only described by the upper parts of the MS curves – while the lower parts (describing *barotropic* instability) can, and do, depend on ΔH. Secondly, the asymptotic results are applicable only to small ε.

Given these reservations, Fig. 5 confirms that, for thin vortices, the criterion of baroclinic instability is effectively independent of the amplitude of the vortex. Indeed, observe that, as $\varepsilon \to 0$, the upper parts of the MS curves with different values of ΔH are all 'bunched' together (as they should be according to the asymptotic predictions of Benilov, 2005).

3.3. Comparison with observations

To place the above results in oceanographic context, we shall plot the computed MS curve together with the 35 rings catalogued in Olson (1991). Unfortunately, this paper provides no data on the depth ratio ε, so we have to assume, on a more or less *ad hoc* basis, that

$$0.05 \lesssim \varepsilon \lesssim 0.1.$$

Thus, each ring in Fig. 6 is represented by an interval with a fixed R, but uncertain ε. Nor does (Olson, 1991) provide explicit information on the vortex amplitude ΔH, but this turns out to be unimportant. To understand why, consider the case where the stability region is the largest, i.e., $\Delta H \to 0$ (QG vortices). However, even for this, most 'favorable' value of ΔH, only 6 out of the 35 vortices are stable – and we conclude that the model of compensated Gaussian vortices cannot account for the observed numbers and longevity of oceanic eddies.

Finally, Fig. 6 shows that none of the 29 unstable vortices fell into the area of *barotropic* instability: their radii are just too large for that.

3.4. Algebraic vortices

To clarify to which extent the above results depend on the vortex's shape, we considered several other vortex profiles, e.g. an algebraic one,

$$H_1 = 1 + \Delta H\left(1 + \frac{r^2}{5R^2}\right)^{-2}, \tag{31}$$

where R and ΔH are, again, the non-dimensional radius and amplitude. Examples of algebraic vortices are shown in Fig. 7. Observe also that, for the algebraic profile, the existence restriction (29) remains intact, whereas the equivalent of restriction (30) is

$$R^2 \geqslant \frac{16}{5}\Delta H. \tag{32}$$

It turns out that almost all conclusions obtained for the Gaussian profile apply to the algebraic one as well, with only two exceptions. Firstly, the latter is barotropically stable – hence, there is no region of barotropic instability for $k = 2$ and the MS curve of this mode looks similar to those for other values of k (see Fig. 8). Sec-

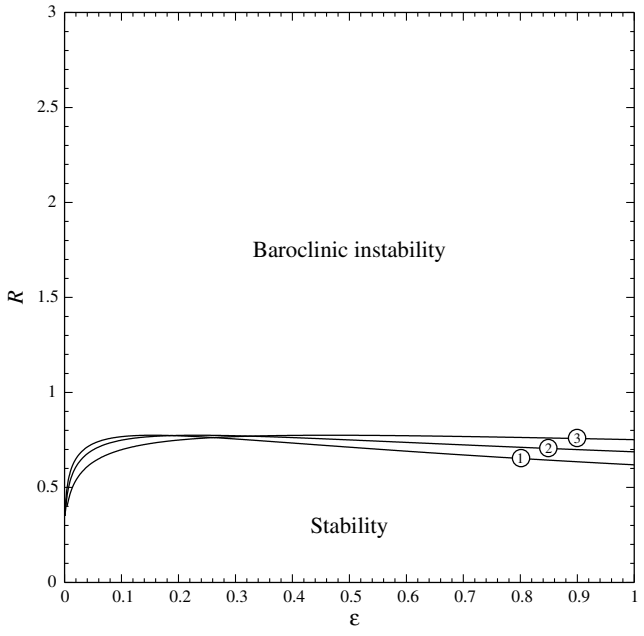

Fig. 8. The stability properties of algebraic quasigeostrophic ($\Delta H \to 0$) vortices. The marginal stability curves are marked with the corresponding values of the azimuthal wavenumber k.

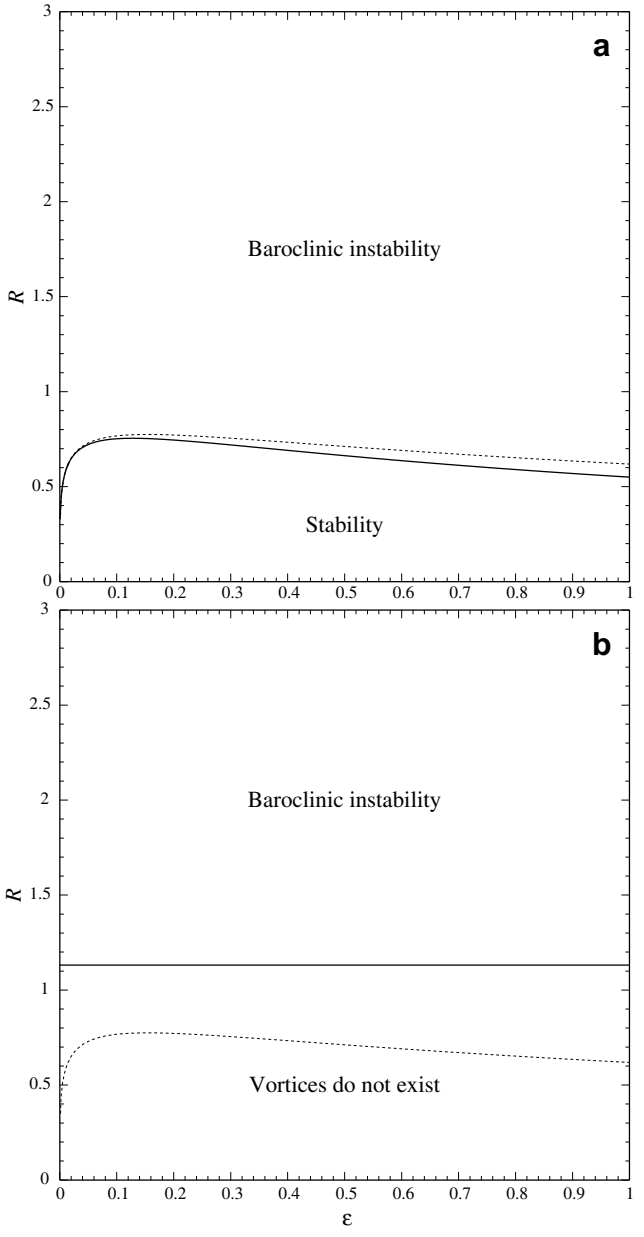

Fig. 9. The marginal stability curve for algebraic ageostrophic vortices, for the first azimuthal mode ($k = 1$). The dotted line shows the corresponding quasigeostrophic ($\Delta H \to 0$) curve. (a) $\Delta H = -0.4$ (cyclones); (b) $\Delta H = 0.4$ (anticyclones), the horizontal line shows constraint (32), and all vortices above it happen to be unstable (i.e., no marginal stability curve exists).

ondly, the region of stability for the algebraic profile is so small that, for $\Delta H \gtrsim 0.2$, no stable vortices exist due to restriction (32) (see Fig. 9 and compare it with Fig. 4).

Thus, algebraic compensated vortices (as well as other vortex profiles considered), cannot account for the observed longevity of oceanic eddies.

4. Vortices with uniform PV in the lower-layer

As shown in Benilov (2005), QG vortices with a lower-layer flow corresponding to uniform PV are much more stable than their compensated counterparts. In the remainder of this paper we shall examine how this conclusion is affected by ageostrophic effects.

The condition that the lower-layer PV is uniform is

$$\frac{\frac{1}{r}\frac{\mathrm{d}}{\mathrm{d}r}(rV_2)+1}{H_2} = \text{const}. \tag{33}$$

Then, conditions (8) indicate that const = 1, whereas (7) and (33) yield

$$H_2 = 1-\varepsilon(H_1-1), \tag{34}$$

$$\frac{\mathrm{d}}{\mathrm{d}r}(rV_2) = -\varepsilon r(H_1-1), \tag{35}$$

respectively. We also impose the obvious boundary condition

$$V_2 \to 0 \quad \text{as} \quad r\to\infty. \tag{36}$$

Eqs. (35) and (36) determine $V_2(r)$ for a given $H_1(r)$. Then, $P_2(r)$ can be computed using

$$\frac{\mathrm{d}P_2}{\mathrm{d}r} = V_2 + \frac{1}{r}V_2^2, \tag{37}$$

which follows from (7). Since an arbitrary constant can always be added to pressure, the boundary condition for P_2 is unimportant, and one can simply put

$$P_2 = 0 \quad \text{at } r=0. \tag{38}$$

Having solved (37) and (38), one can find

$$P_1 = P_2 + H_1 \tag{39}$$

and, eventually,

$$V_1 = \frac{1}{2}\left(\sqrt{r^2+4r\frac{\mathrm{d}P_1}{\mathrm{d}r}}-r\right). \tag{40}$$

For a Gaussian $H_1(r)$, vortices with uniform PV in the lower-layer [described by (34)–(40)] are shown in Fig. 10. One can see that, in the 'core' of the vortex, V_2 is noticeably smaller than V_1 (it follows from (35) that the former scales with the depth ratio ε, which is usually small). At the periphery of the vortex, as follows from (34) to (40),

$$V_{1,2} \to -\frac{\varepsilon M}{r} \quad \text{as} \quad r\to\infty, \tag{41}$$

where

$$M = \int_0^\infty r(H_1-1)\mathrm{d}r$$

is the net mass anomaly of the vortex. Thus, vortices with uniform lower-layer PV decay at infinity much slower than their compensated counterparts.

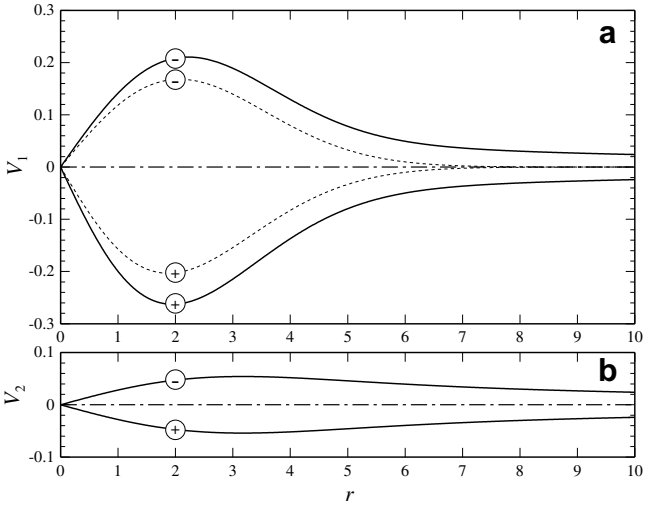

Fig. 10. Examples of Gaussian vortices with uniform lower-layer PV, (34)–(40), with $\Delta H = \pm 0.6$, $R = 2$, $\varepsilon = 0.1$ (the cyclone/anticyclone are marked with −/+, respectively). (a) $V_1(r)$, dotted line shows the compensated vortex with the same parameters; (b) $V_2(r)$.

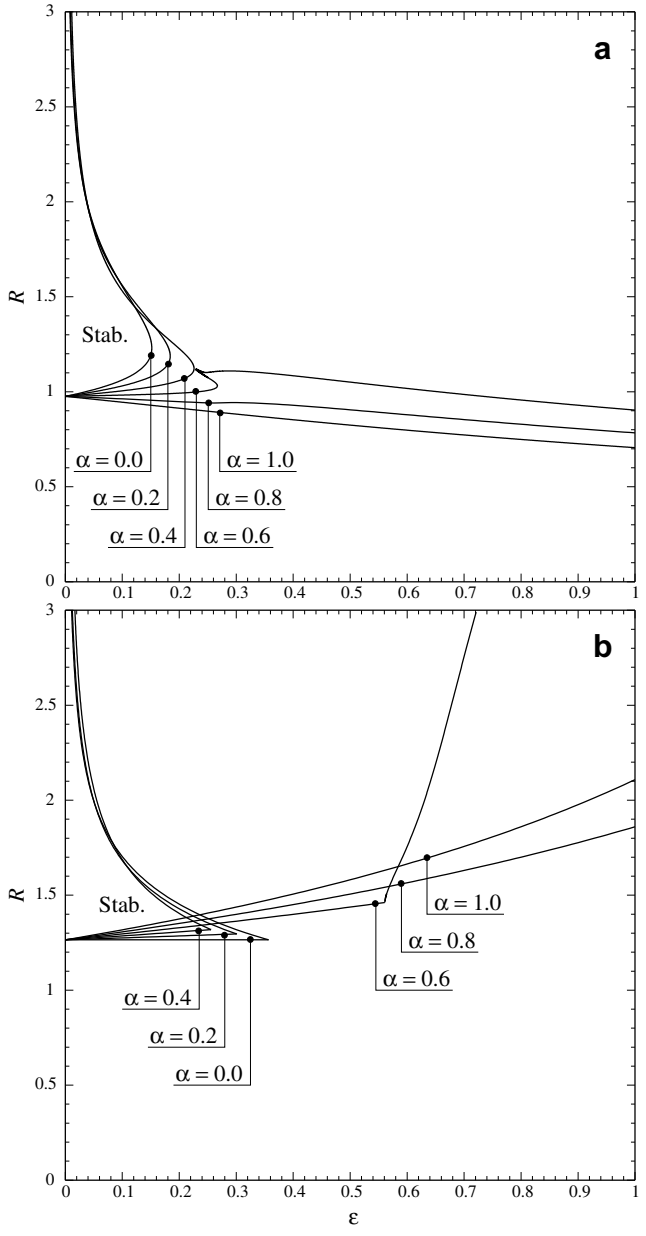

Fig. 11. The marginal instability curves (corresponding to $\mathrm{Im}\omega = 10^{-4}$) for Gaussian vortices with deep flow, for the second azimuthal mode ($k = 2$), for $\alpha = 0$, 0.2, 0.4, 0.6 where α is defined by (42). (a) Cyclones with $\Delta H = -0.4$; (b) anticyclones with $\Delta H = 0.4$.

4.1. Numerical results and comparison with observations

In order to trace the change in MS curves with transition from compensated vortices to those with uniform PV in the lower-layer, assume that

$$V_2 = \alpha (V_2)_{\mathrm{uPV}}, \tag{42}$$

where $(V_2)_{\mathrm{uPV}}$ is the solution of the uniform PV Eqs. (35) and (36), and α is a number between 0 (compensated vortex) and 1 (uniform PV in the lower-layer). For the remainder of this paper, we shall confine ourselves to Gaussian vortices, with $H_1(r)$ given by (28).

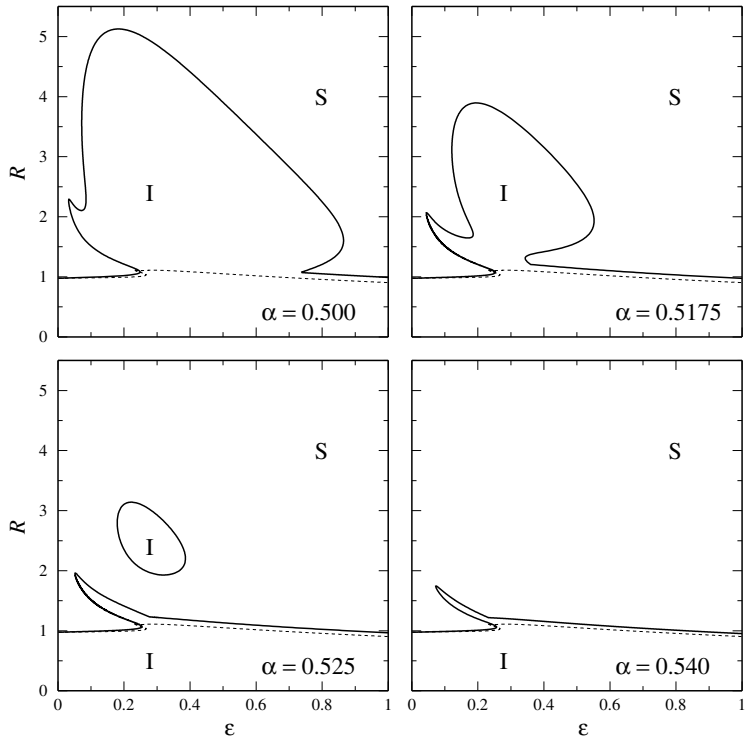

Fig. 12. The marginal instability (MI) curves for Gaussian vortices with deep flow, for the second azimuthal mode ($k = 2$), for $\Delta H = -0.4$ (cyclones) and various values of α. A 'reference' MI curve, corresponding to $\alpha = 0.6$, is shown in dotted line. The stability/instability regions are marked with an S/I.

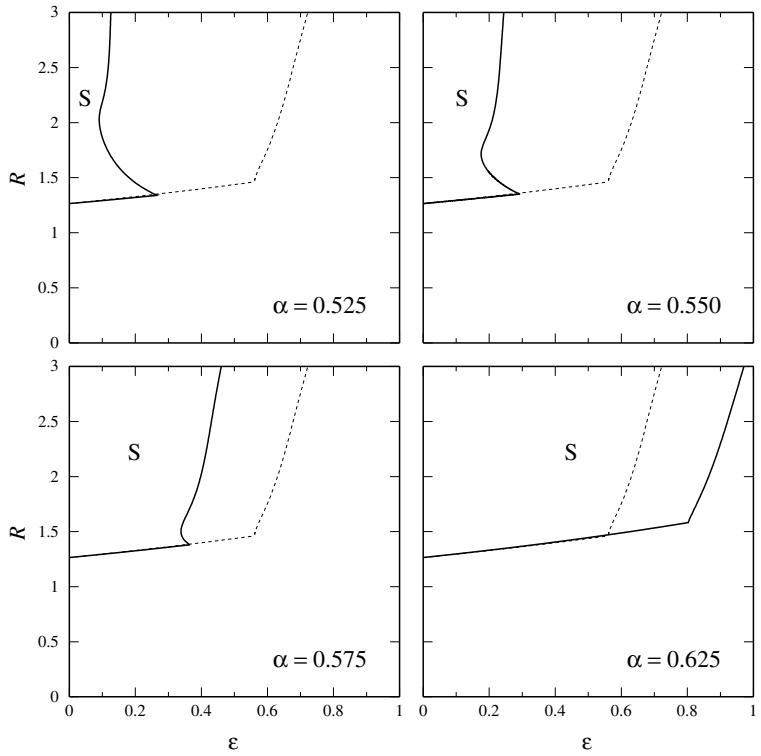

Fig. 13. The same as in Fig. 12, but for $\Delta H = 0.4$ (anticyclones).

Note that, for $\alpha \neq 0$, the existence restriction [guaranteeing that (40) yields a real $V_1(r)$] has no obvious analytical representation, but can be readily computed.

It turns out that, for $\alpha \lesssim 0.4$, the MS curves are virtually the same as those for compensated vortices. The growth rates, however, are significantly lower, giving rise to 'strips' of weakly unstable vortices adjacent to the MS curves. By $\alpha \sim 0.5$, these strips become very wide, with the (non-dimensional) growth rate being extremely small ($\sim 10^{-7} - 10^{-8}$) – as a result, the exact location of the MS curve is very difficult to spot. Physically, such a weak instability is indistinguishable from stability, which makes MS curves irrelevant.

Therefore, instead of marginal stability curves, we shall use the curves in the (ε,R)-plane such that

$$\mathrm{Im}\omega = 10^{-4}. \tag{43}$$

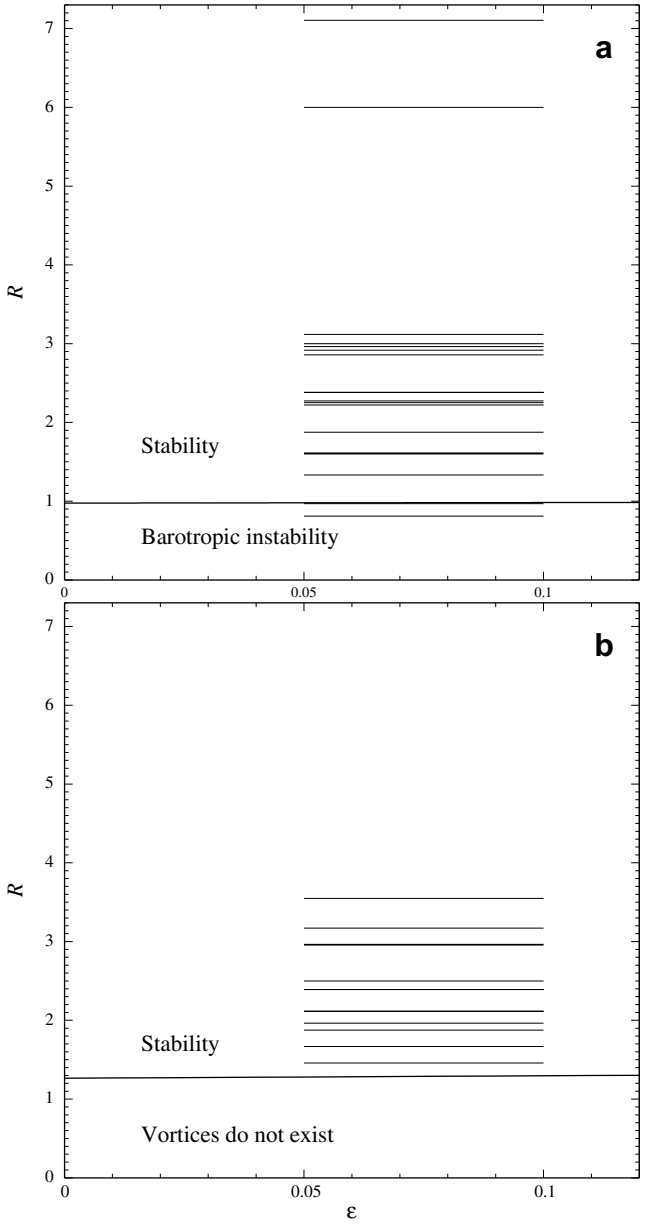

Fig. 14. The marginal instability curve for Gaussian vortices with deep flow, for the second azimuthal mode ($k = 2$), for $\alpha = 0.6$. Horizontal segments show the parameters of rings catalogued in Olson (1991). (a) Cyclones with $\Delta H = -0.4$; (b) anticyclones with $\Delta H = 0.4$.

Recalling that the time variable is non-dimensionalized using the Coriolis parameter f_0, and estimating f_0 for a latitude of 45°, one can see that (43) corresponds to the characteristic time of instability $(f_0 \mathrm{Im}\omega)^{-1}$, being more than 3 years. Curves (43) will be referred to as marginal *in*stability (MI) curves.

Fig. 11 shows the MI curves for various α. Interestingly, stabilization does *not* occur gradually over the whole interval $0 < \alpha < 1$, but mainly between $\alpha \approx 0.5$ and $\alpha \approx 0.6$. This effect is illustrated in Figs. 12 and 13, which are the two most important figures of this paper. One can see that, by $\alpha = 0.6$, the MI curves 'unfold' (for cyclones) or 'expand' (for anticyclones), and the stability region 'opens up', i.e., all vortices above the MI curves are virtually stable.

Note also that the 'corners' of the curves shown in Figs. 12 and 13 are of different origin. In the latter (i.e., for anticyclones), corners represent junctions of the MI curves and the existence curves. In Fig. 12 (i.e., for cyclones), on the other hand, corners correspond to points, where two different modes (existing for the same value of the azimuthal wavenumber k) merge – this feature has been observed only for non-compensated cyclones, and only within a narrow range of α.

Finally, Fig. 14 shows that, for $\alpha = 0.6$, model (42) predicts that 33 out the 35 eddies catalogued in Olson (1991) are virtually stable. Note that the two unstable cyclones (shown in Fig. 14a) cannot be stabilized by a further increase in α, as they are subject to *barotropic* instability, which is effectively independent of the deep flow. If, however, the MI curves in Fig. 14 were computed for a smaller vortex amplitude, say $\Delta H = 0.2$, the two unstable eddies would also fall into the region of virtual stability. Since (Olson, 1991) does not provide tangible information on the thicknesses of the eddies catalogued there, we shall not discuss this issue in further detail.

5. Ripa's stability criterion

When dealing with ageostrophic vortices, one can, in principle, take advantage of a sufficient stability criterion derived by Ripa (1989, 1991) – but, surprisingly, no-one has actually done this. The reason for that is as follows: Ripa's criterion turns out to be so restrictive that it does not hold for any oceanic vortices with realistic parameters.

Indeed, let us adapt the axisymmetric version of Ripa's criterion for the two-layer ocean, which yields

$$\left(\frac{1}{r}V_j - \Omega\right)\frac{\mathrm{d}Q_j}{\mathrm{d}r} > 0 \quad \text{for all} \quad r > 0, \tag{44}$$

$$\frac{\left(\frac{1}{r}V_1 - \Omega\right)^2 r^2}{H_1} + \frac{\varepsilon\left(\frac{1}{r}V_2 - \Omega\right)^2 r^2}{H_2} < 1 \quad \text{for all} \quad r > 0, \tag{45}$$

where

$$Q_j = \frac{1}{H_j}\left(1 + \frac{1}{r}V_j + \frac{\mathrm{d}V_j}{\mathrm{d}r}\right) \tag{46}$$

is the non-dimensional potential vorticity of the jth layer and Ω is an arbitrary constant. Note that condition (44) must hold for both layers, i.e., $j = 1,2$.

First of all, observe that, as $r \to \infty$, the left-hand side of inequality (45) grows as $\Omega^2 r^2$, whereas the right-hand side remains bounded. Hence, (45) can hold only if

$$\Omega = 0. \tag{47}$$

Then, substitution of (46) and (47) into (44) yields

$$V_j\left[\frac{1}{H_j}\left(-\frac{1}{r^2}V_j + \frac{1}{r}\frac{\mathrm{d}V_j}{\mathrm{d}r} + \frac{\mathrm{d}^2V_j}{\mathrm{d}r^2}\right) - \frac{1}{H_j^2}\frac{\mathrm{d}H_j}{\mathrm{d}r}\left(1 + \frac{1}{r}V_j + \frac{\mathrm{d}V_j}{\mathrm{d}r}\right)\right] > 0. \tag{48}$$

Now, assume that

$$\frac{dH_1}{dr} > 0, \quad V_1 > 0 \quad \text{for all} \quad r > 0, \tag{49}$$

i.e., we consider a cyclone with a monotonic profile of the interface. We shall also introduce the point of extreme (maximum) velocity, $r = r_{ext}$, where

$$\frac{dV_1}{dr} = 0, \quad \frac{d^2V_1}{dr^2} < 0 \quad \text{at} \quad r = r_{ext}. \tag{50}$$

Then, by virtue of (49) and (50), condition $(48)_{j=1}$ cannot hold at $r = r_{ext}$, as both terms on the left-hand side are strictly negative.

Next, assume that

$$\frac{dH_1}{dr} < 0, \quad V_1 < 0 \quad \text{for all} \quad r > 0, \tag{51}$$

i.e., we consider an anticyclone (again, with a monotonic profile). At the point of extreme velocity, we have

$$\frac{dV_1}{dr} = 0, \quad \frac{d^2V_1}{dr^2} > 0 \quad \text{at} \quad r = r_{ext}. \tag{52}$$

Then, if the flow in the upper-layer is not too strong, namely,

$$\frac{1}{r_{ext}}|V_j(r_{ext})| \leqslant 1, \tag{53}$$

one can clearly see that, by virtue of (52) and (53), condition $(48)_{j=1}$ cannot hold at $r = r_{ext}$.

Note that, dimensionally, condition (53) implies that the angular velocity at $r = r_{ext}$ is smaller than the Coriolis parameter. If, for example, the radius of maximum velocity is 30 km (which is close to the lower estimate for this characteristic) and the latitude is 45°, (53) requires that the dimensional velocity of the vortex is less than 3 m/s, which holds for all conceivable oceanic vortices.

We conclude that Ripa's stability criterion does not hold for the Earth's ocean (which does not imply, however, that no stable vortices exist there, as this criterion is not a necessary one).

6. Concluding remarks

Thus, we have examined how ageostrophic effects influence the stability of vortices in a two-layer ocean. Two models were examined: compensated vortices (with no flow in the lower-layer) and those with a 'deep' flow such that the lower-layer PV is uniform.

The following conclusions were obtained:

- *Large* compensated vortices, with radii exceeding the deformation radius by a factor of 2–3, are *baroclinically* unstable. For the most important limit of thin vortices, the corresponding marginal stability (MS) curves are independent of the vortex amplitude, i.e., ageostrophic affects are unimportant in this case.
- *Small* compensated *cyclones*, with radii smaller than the deformation radius, are unstable *barotropically*, and ageostrophic effects make the instability stronger. As a result, stable compensated cyclones exist for a fairly limited range of radii. The allowable range of the radii of small compensated *anticyclones* is bounded below by either barotropic instability (for small amplitudes) or an existence condition guaranteeing that the Coriolis force can hold the vortex together by balancing the centrifugal force and pressure gradient (for large amplitudes). One way or another, very few 'real' oceanic eddies, both cyclones and anticyclones, fall into the allowable range (generally, their radii are just too large).
- The stability properties of *small* vortices with uniform PV in the lower-layer are approximately the same as those of compensated vortices, with respect to both barotropic instability and non-existence due to strong centrifugal force and/or pressure gradient.
- The stability properties of *large* vortices with uniform lower-layer PV are completely different to what was observed for their compensated counterparts, as the former are stable for all amplitudes. As a result, most if not all observed eddies 'fit' into the range of theoretically stable vortices.

Note that the above conclusions refer to *linear* stability of vortices and, thus, ignore nonlinear effects – which, in principle, can provide an alternative mechanism of vortex stabilization. In the QG case, for example, linearly unstable vortices can stabilize when the disturbance reaches a certain amplitude (Flierl, 1988; Helfrich and Send, 1988; Carton and McWilliams, 1996; Correard and Carton, 1999). In ageostrophic models, nonlinear effects can stabilize circular vortices as ellipses (Dewar et al., 1999) or tripoles (Baey and Carton, 2002). It would be interesting to see how these nonlinear models fare for the parameters of 'real' oceanic eddies catalogued in Olson (1991).

Another restriction of our conclusions results from the two-layer model used to obtain them. Indeed, intra-thermocline eddies (such as Mediterranean meddies, for example) should rather be described by a *three*-layer model, with a relatively thin middle layer (where the vortex is localized) 'sandwiched' by two thicker layers. Furthermore, the problem of vortex stability should eventually be examined using the *continuous* approximation of the ocean, which combines the advantages of higher resolution of the vertical structure of the flow with proper representation of critical levels.

References

Baey, J.M., Carton, X., 2002. Vortex multipoles in two-layer rotating shallow-water flows. J. Fluid Mech. 460, 151–175.

Benilov, E.S., Broutman, D., Kuznetsova, E.P., 1998. On the stability of large-amplitude vortices in a continuously stratified fluid on the f-plane. J. Fluid Mech. 355, 139–162.

Benilov, E.S., 2003. Instability of quasigeostrophic vortices in a two-layer ocean with thin upper layer. J. Fluid Mech. 475, 303–331.

Benilov, E.S., 2004. Stability of vortices in a two-layer ocean with uniform potential vorticity in the lower layer. J. Fluid Mech. 502, 207–232.

Benilov, E.S., 2005. The effect of ageostrophy on the stability of vortices in a two-layer ocean with thin upper layer. Dyn. Atmos. Oceans 39, 211–226.

Carton, X.J., McWilliams, J.C., 1989. Barotropic and baroclinic instabilities of axisymmetric vortices in a quasigeostrophic model. In: Nihoul, J.C.J., Jamart, B.M. (Eds.), Mesoscale/Synoptic Coherent Structures in Geophysical Turbulence: Proceedings of the 20th International Liège Colloquium on Ocean Hydrodynamics, Elsevier Oceanography Series, vol. 50. Elsevier, Amsterdam, p. 225.

Carton, X.J., McWilliams, J.C., 1996. Nonlinear oscillatory evolution of a baroclinically unstable geostrophic vortex. Dyn. Atmos. Oceans 24, 207–214.

Correard, S., Carton, X.J., 1999. Formation and stability of tripolar vortices in stratified geostrophic flows. Il Nuovo Cimento C 22, 767–777.

Dewar, W.K., Killworth, P.D., 1995. On the stability of oceanic rings. J. Phys. Oceanogr. 25, 1467–1487.

Dewar, W.K., Blundell, J.R., Killworth, P.D., 1999. Primitive equation instability of wide oceanic rings Part 2: numerical studies of ring stability. J. Phys. Oceanogr. 29, 1744–1785.

Flierl, G.R., 1988. On the instability of geostrophic vortices. J. Fluid Mech. 197, 349–388.

Helfrich, K.R., Send, U., 1988. Finite-amplitude evolution of two-layer geostrophic vortices. J. Fluid Mech. 197, 331–348.

Ikeda, M., 1981. Instability and splitting of mesoscale rings using a two-layer quasi-geostrophic model on an f-plane. J. Phys. Oceanogr. 11, 987–998.

Katsman, C.A., Van der Vaart, P.C.F., Dijkstra, H.A., de Ruijter, W.P.M., 2003. Stability of multi-layer ocean vortices: a parameter study including realistic Gulf Stream and Agulhas rings. J. Phys. Oceanogr. 33, 1197–1218.

Killworth, P.D., Blundell, J.R., Dewar, W.K., 1997. Primitive equation instability of wide oceanic rings. Part 1: linear theory. J. Phys. Oceanogr. 27, 941–962.

Lai, D.Y., Richardson, P.L., 1977. Distribution and movement of Gulf Stream rings. J. Phys. Oceanogr. 7, 670–683.

Olson, D.B., 1991. Rings in the ocean. Ann. Rev. Earth Planet. Sci. 19, 283–311.

Ripa, P., 1989. On the stability of ocean vortices. In: Nihoul, J.C.J., Jamart, B.M. (Eds.), Mesoscale/Synoptic Coherent Structures in Geophysical Turbulence: Proceedings of the 20th International Liège Colloquium on Ocean Hydrodynamics, Elsevier Oceanography Series, vol. 50. Elsevier, Amsterdam, p. 167.

Ripa, P., 1991. General stability conditions for a multi-layer model. J. Fluid Mech. 222, 119–137.

Ripa, P., 1992. Instability of a solid-body rotating vortex in a two-layer model. J. Fluid Mech. 242, 395–417.